Semicond. Sci. Technol. 10 (1995) 260–269. Printed in the UK

Inelastic and elastic mechanisms of electron capture to a quantum well

Dennis Bradt, Yuri M Sirenko† and Vladimir Mitin

Department of Electrical and Computer Engineering, Wayne State University, Detroit, MI 48202, USA

Received 6 December 1994, accepted for publication 5 January 1995

Abstract. We present a calculation of electron capture rates to a single quantum well (QW) taking full account of the quasibound 2D states, which are localized in the vicinity of a QW at energies above the barrier. To find the net capture rates we calculate the rates of capture, escape and carrier relaxation within the bound 2D states, assisted by both emission and absorption of optical phonons by an electron with arbitrary positive initial energy, as well as (quasi)elastic impurity and acoustic phonon scattering. The dependences of the capture rates of the non-degenerate electrons on the well width and temperature are discussed.

1. Introduction

The mechanism for carrier capture to a quantum well (QW) is of fundamental importance to the understanding of the vertical transport and luminescence in semiconductor structures with quantum confinement. The capture of electrons plays a key role in defining the ultimate performance of many modern QW devices, in particular QW lasers [1] and infrared photodetectors [2].

In the first works the processes of carrier capture to QW were treated semiclassically [3] as carrier diffusion in a separate confinement region. Later Brum and Bastard [4] performed quantum mechanical calculations for LO phonon-assisted electron capture to a single QW and predicted the oscillation of capture time versus width of the well due to resonances associated with the appearance of new states in the QW. Their results were extended in subsequent works by consideration of graded-index separate confinement heterostructures [5], interaction with the quantized optical phonon modes in superlattices [6], indirect capture via bound states of the barrier impurities [7], electron–electron interaction and screening [8], capture of holes to QW with allowance for a complex structure of the valence band [9], Coulomb attraction between captured electron and holes [10], spatial decay of the electron wavefunction due to a strong scattering [11] and calculations of electron capture rates to quantum wires and dots [12].

Until recently the observed capture times seemed to contradict the predictions of the quantum mechanical model. Picosecond time-resolved [13] and continuous-wave [14] photoluminescence measurements gave capture rates which did not agree with the theoretical calculations and no resonant well width dependence was observed. However, in the latest subpicosecond pump and probe photoluminescence experiments, the *resonant* capture of an electron to a QW has been observed and predictions of the quantum mechanical model were confirmed for sufficiently thin (< 300 Å) wells [15, 16]. The observation of the resonant features of the capture process became possible in part due to special techniques which enhance the quantum mechanical reflectivity of the electron (use of thin tunnel barriers on both sides of the well) and eliminate the relaxation processes that obscure the observation of capture (resonant excitation of carriers to the bottom of the barrier).

Since the pioneering paper by Brum and Bastard [4] the majority of works have treated electron capture as the transition from unbound three-dimensional (3D) states to the truly bound two-dimensional (2D) states in a well with energy below the barrier, $E < 0$. Thus, at low electron concentration, only electrons with energies in the range $0 < E < \hbar\omega_0$ can be captured after the emission of an optical phonon of energy $\hbar\omega_0$. Only a few publications [16–20] have considered an alternative capture mechanism via quasibound 2D states having total energies above the barrier, because of the large in-plane kinetic energy.

Lent and Porod [18] have analysed the matrix elements for the electron escape rates from the QW and suggested that a different dependence on the transferred momentum q under certain conditions can lead to suppression of scattering by polar optical phonons relative to non-polar optical and acoustic phonon scattering. On the other hand, in [16] the results of femtosecond time-resolved luminescence measurements of carrier capture to multi-quantum well structures were interpreted in terms of the competing influence of LO

† Present address: Department of Electrical and Computer Engineering, North Carolina State University, Raleigh, NC 27695, USA.

0268-1242/95/030260+10$19.50

phonon scattering and impurity scattering. Calculation of capture rates due to interface impurity scattering has shown that the latter can dominate when the LO phonon scattering reveals resonant minima. Recently Weber and Paula [20] showed that the partial excitation of electrons to the quasibound states during the luminescence experiments could result in faster relaxation and capture.

In this paper we present an analysis of the electron capture to a QW with the participation of the quasibound 2D states, which are localized in the vicinity of a QW at energies above the barrier. We calculate the rates of capture assisted by both emission and absorption of optical phonons by an electron with arbitrary positive initial energy, as well as (quasi)elastic impurity and acoustic phonon scattering.

The rest of the paper is organized as follows. In section 2 we formulate the model and write the basic equations. In section 3 we present expressions for the rates of all possible transitions of electrons (capture, escape and intersubband transitions) due to inelastic and elastic scattering. Section 4 contains the results of numerical calculations and discussion. The expressions for the form factors of the transitions are presented in the appendix.

2. Model and basic equations

We consider a single rectangular quantum well with the potential $V(r) = -V_0$ for $-a/2 < z < a/2$ and $V(r) = 0$ otherwise (see figure 1). We assume the difference between the effective masses in the well and barriers to be small and set the effective mass m to be constant over the whole space.

The electron wavefunctions $\Psi(r)$ are characterized, in addition to the wavevector $k_\parallel$ in the xy plane, by the discrete quantum number n for the states localized in the vicinity of the well, or by quantum numbers k_z and p for unbound states in the parity representation:

$$\Psi_{k_\parallel,n}(r) = \mathcal{S}^{-1/2}\exp(ik_\parallel r_\parallel)\psi_n(z) \quad (1)$$

$$\Psi_{k_\parallel,k_z,p}(r) = \mathcal{S}^{-1/2}\exp(ik_\parallel r_\parallel)\psi_{k_z,p}(z). \quad (2)$$

Here $\mathcal{S}$ is a normalization area; $n = 0, 1, \ldots$ numbers the quantum subbands in the well and p is the the parity of unbound state ($p = 0$ for a symmetric state and $p = 1$ for the antisymmetric one). In the parity representation the wavevector k_z can be chosen to be positive, $k_z > 0$.

Corresponding eigenenergies are given by

$$E_{k_\parallel,n} = \frac{\hbar^2}{2m}(-\kappa_n^2 + k_\parallel^2) \equiv \frac{\hbar^2}{2m}(\kappa_{wn}^2 + k_\parallel^2) - V_0 \quad (3)$$

$$E_{k_\parallel,k_z,p} = \frac{\hbar^2}{2m}(k_z^2 + k_\parallel^2) \equiv \frac{\hbar^2}{2m}(k_{wz}^2 + k_\parallel^2) - V_0. \quad (4)$$

Thus, $\epsilon_n = \hbar\kappa_n^2/2m$ is the ionization energy of the nth subband; the variables κ_{wn} and k_{wz} (the subscript w stands for 'well') are defined by the right-hand sides of equations (3) and (4). The eigenvalues for the bound states are found from the following transcendental equation:

$$\tan\frac{a\kappa_{wn} + \pi n}{2} = \sqrt{2mV_0/\hbar^2\kappa_{wn}^2 - 1}.$$

With the help of the notation

$$\mathrm{cs}_n(x) = \begin{cases} \cos x & \text{for even } n \\ \sin x & \text{for odd } n \end{cases}$$

the transverse wavefunctions of bound states can be written as

$$\psi_n(z) = C_n \times \begin{cases} (\mathrm{sgn}\, z)^n \exp[\kappa_n(a/2 - |z|)] & \text{for } |z| > a/2 \\ \mathrm{cs}_n(\kappa_{wn}z)/\mathrm{cs}_n(\kappa_{wn}a/2) & \text{for } |z| < a/2. \end{cases} \quad (5)$$

where the normalization constant is

$$C_n = \left(\frac{a}{2} + (-1)^n\frac{\sin(\kappa_{wn}a)}{2\kappa_{wn}} + \frac{\mathrm{cs}_n^2(\kappa_{wn}a/2)}{\kappa_n}\right)^{-1/2} \times \mathrm{cs}_n(\kappa_{wn}a/2).$$

For unbound states we have

$$\psi_{k_z,p}(z) = \sqrt{\frac{2}{\mathcal{L}}} \times \begin{cases} \mathrm{cs}_p[k_z(|z| - a/2) + \varphi_p] & \text{for } |z| > a/2 \\ \dfrac{\mathrm{cs}_p(\varphi_p)}{\mathrm{cs}_p(k_{wz}a/2)}\mathrm{cs}_p(k_{wz}z) & \text{for } |z| < a/2 \end{cases} \quad (6)$$

where the phase φ_p is found from the equation

$$\tan\varphi_p = (k_{wz}/k_z)^{1-2p}\tan(k_{wz}a/2)$$

and $\mathcal{L}$ is a normalization length in the z-direction.

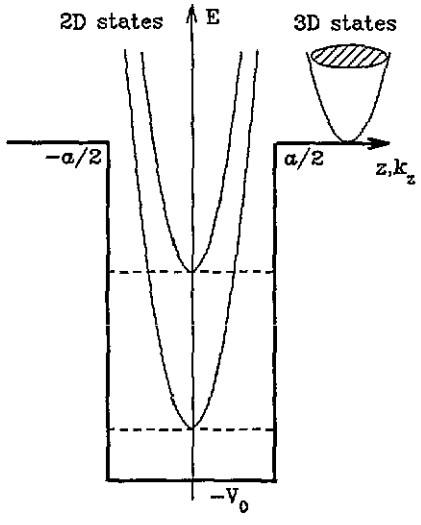

Figure 1. Geometry of the system—finite rectangular quantum well of width a and depth V_0. Two-dimensional (confined) states and three-dimensional (extended) states are shown schematically.

The net electron capture rate to a quantum well is specified by the combination of capture, escape, relaxation through the confined 2D states, and radiative recombination with the holes at the bottom of the QW. Below we consider the case of a small electron concentration and we will neglect the influence of electron–electron scattering. Moreover, we assume that the recombination is fast enough to prevent filling of the confined states.

In this case, the net capture rate is equal to the rate of transition from the 3D to 2D states multiplied by the probability of a recently captured electron relaxing down through the confined states instead of being re-emitted to the 3D states. Therefore, in addition to the capture rate, the rates of relaxation within 2D states and escape should be calculated.

Since even at positive energies there exist 2D-like 'quasibound' states with a large kinetic energy of the in-plane motion, the capture to QW is not limited by emission of an LO phonon by an electron with an initial energy below $\hbar\omega_0$. Electrons with any energy can emit or *absorb* the phonon, or be scattered elastically to quasibound states with the energies above the barrier. In the second stage such 'pseudocaptured' electrons can relax effectively to the bottom of QW due to emission of LO phonons.

In the following we consider the electron transitions due to scattering by LO and DA phonons as well as impurities localized at the interfaces. Transition probabilities can be written in the form

$$W_{i\to f}^{(q)} = \frac{2\pi}{\hbar}\left|\langle\Psi_i(\boldsymbol{r})\,|\,V(\boldsymbol{r})|\,\Psi_f(\boldsymbol{r})\rangle\right|^2\delta(E_f - E_i \pm \hbar\omega_q) \tag{7}$$

where i and f are initial and final electron states: for electron capture $i \equiv (\boldsymbol{k}_\parallel, k_z, p)$ and $f \equiv (\boldsymbol{k}'_\parallel, n)$; for escape $i \equiv (\boldsymbol{k}_\parallel, n)$ and $f \equiv (\boldsymbol{k}'_\parallel, k_z, p)$; for transitions within 2D states $i \equiv (\boldsymbol{k}_\parallel, n)$ and $f \equiv (\boldsymbol{k}'_\parallel, n')$. In the case of phonon scattering $\boldsymbol{q}$ is a phonon wavevector, the upper sign corresponds to the emission, and the lower sign to the absorption of a phonon.

To calculate the rates due to polar optical phonon scattering we use equation (7) with $\omega_q = \omega_0$ and

$$V_{\mathrm{LO}}(\boldsymbol{r}) = \left[2\pi e^2\hbar\omega_0 N^{\pm}(\omega_0)/\varepsilon^* q^2 \mathcal{S}\mathcal{L}\right]^{1/2}\exp(i\boldsymbol{q}\boldsymbol{r}). \tag{8}$$

Here $N^{\pm}(\omega_q) = [\exp(\hbar\omega_q/T) - 1]^{-1} + 1/2 \pm 1/2$ is a phonon occupation factor and T is a lattice temperature; $1/\varepsilon^* \equiv 1/\varepsilon_\infty - 1/\varepsilon_0$, where ε_0 and ε_∞ are static and high-frequency dielectric susceptibilities of the crystal.

For deformation acoustic phonon scattering we have $\omega_q = sq$, and V_{DA} is given by equation (8) after changing $2\pi e^2/\varepsilon^* q^2$ to $\hbar D^2 q/2\rho s$, where s, D and ρ are the sound velocity, deformation potential constant and crystal density respectively. Below we use the quasielastic approximation, setting $\omega_q \to 0$ and

$$V_{\mathrm{DA}}(\boldsymbol{r}) = \sqrt{D^2 T/2\rho s^2 \mathcal{L}\mathcal{S}}\exp(i\boldsymbol{q}\boldsymbol{r}) \tag{9}$$

for both emission and absorption of an acoustic phonon.

In the case of elastic scattering by uncorrelated impurities with a sheet concentration n_i located at the interface ($z = a/2$) we use equation (7) with $\omega_q = 0$ and

$$V_{\mathrm{imp}}(\boldsymbol{r}) = \sqrt{n_i \mathcal{S}}\, e^2/\varepsilon_0\sqrt{x^2 + y^2 + (z - a/2)^2}. \tag{10}$$

On the basis of expression (7) for the transition probability between given microscopic initial and final states, we define three transition rates corresponding to a less detailed description of the scattering processes.

The scattering rate from the given microscopic initial state i is equal to

$$W_i = \sum_f \left(\sum_q\right) W_{i\to f}^{(q)} \tag{11}$$

where for impurity scattering the summation over q should be ignored.

We also define the averaged transition probability per unit initial energy,

$$\frac{\partial W}{\partial E} = \sum_i \sum_f \left(\sum_q\right) W_{i\to f}^{(q)}\delta(E - E_i). \tag{12}$$

Finally, the total transition rate can be obtained from equation (11) or (12),

$$\begin{aligned} W &= 2\sum_i f(E_i)[1 - f(E_i \mp \hbar\omega_q)]W_i \\ &= 2\int f(E)[1 - f(E \mp \hbar\omega_q)]\frac{\partial W}{\partial E}\,\mathrm{d}E \end{aligned} \tag{13}$$

where $f(E)$ is a distribution function of the electron gas.

3. Transition rates

In this section we calculate the capture rates from a microscopic initial state W_i, transition rates per unit energy $\partial W/\partial E$, and total transition rates W, for LO and DA phonon and impurity scattering.

3.1. Capture rates from a given initial state

For LO phonon scattering, we find from equations (7), (8) and (11) the following capture rate:

$$\begin{aligned} \left(W_{k_\parallel, k_z, p}\right)_{3\mathrm{D}\to 2\mathrm{D}}^{\mathrm{LO}} &= \frac{4e^2 m\omega_0}{\varepsilon^*\hbar^2\mathcal{L}} N^{\pm}(\omega_0) \\ &\times \int_0^\infty \mathrm{d}q_z \sum_{n,p}{}' \frac{|M_{k_z, p\to n}^{q_z}|^2}{\sqrt{(\pm k_{\mathrm{ph}}^2 - k_z^2 - q_z^2 - \kappa_n^2)^2 + (2q_z k_\parallel)^2}} \end{aligned} \tag{14}$$

where $k_{\mathrm{ph}}^2 = 2m\omega_0/\hbar$. The prime over the sum means that summation is performed only over subbands

satisfying the condition $E + \epsilon_n > \pm\hbar\omega_0$. The form factors

$$M^{q_z}_{k_z,p\to n} = \sqrt{\frac{\mathcal{L}}{2}} \int_{-\infty}^{\infty} \mathrm{d}z\, \psi_{k_z,p}(z)(\cos q_z z + \sin q_z z)\psi_n(z) \tag{15}$$

are given by equation (A1) of the appendix.

In the elastic approximation the capture rates due to the absorption and emission of DA phonons are equal and given by

$$\left(W_{k_\parallel,k_z,p}\right)^{\mathrm{DA}}_{3\mathrm{D}\to 2\mathrm{D}} = \frac{mD^2T}{2\rho s^2\hbar^3\mathcal{L}} \sum_{n,p} \mathcal{A}_{k_z,p\to n} \tag{16}$$

where

$$\mathcal{A}_{k_z,p\to n} \equiv \frac{2}{\pi} \int_0^{\infty} \mathrm{d}q_z \left|M^{q_z}_{k_z,p\to n}\right|^2$$
$$= \mathcal{L} \int_{-\infty}^{\infty} \mathrm{d}z\, |\psi_{k_z,p}(z)|^2 |\psi_n(z)|^2 \tag{17}$$

is calculated in the appendix.

The capture rate due to scattering by interface impurities with a sheet concentration n_i is obtained from equations (7), (10) and (11) and is equal to

$$\left(W_{k_\parallel,k_z,p}\right)^{\mathrm{imp}}_{3\mathrm{D}\to 2\mathrm{D}} = \frac{16\pi m e^4 n_i}{\varepsilon_0^2\hbar^3\mathcal{L}}$$
$$\times \sum_{n,p} \int_{\kappa_-}^{\kappa_+} \frac{\kappa\,\mathrm{d}\kappa}{\sqrt{(\kappa_+^2-\kappa^2)(\kappa^2-\kappa_-^2)}} \left|\frac{\mathcal{I}^{\kappa}_{k_z,p\to n}}{\kappa}\right|^2 \tag{18}$$

where $\kappa_\pm = \sqrt{k_\parallel^2 + k_z^2 + \kappa_n^2} \pm k_\parallel$ and the form factors

$$\mathcal{I}^{\kappa}_{k_z,p\to n} = \sqrt{\frac{\mathcal{L}}{2}} \int_{-\infty}^{\infty} \mathrm{d}z\, \psi_{k_z,p}(z) \exp(-\kappa|z - W/2|)\psi_n(z) \tag{19}$$

are calculated in the appendix (see equation (A3)).

3.2. Energy-dependent rates

Comparison of equations (7), (11) and (12) gives the following expression for the averaged capture rate per unit energy, $\partial W/\partial E$, in terms of the rate $W_{k_\parallel,k_z,p}$:

$$\left(\frac{\partial W}{\partial E}\right)_{3\mathrm{D}\to 2\mathrm{D}} = \frac{m\mathcal{S}\mathcal{L}}{(2\pi\hbar)^2} \int_0^k \mathrm{d}k_z\, W_{k_\parallel=\sqrt{k^2-k_z^2},k_z,p} \tag{20}$$

where $k^2 = 2mE/\hbar^2$.

The escape rates due to the interaction with LO phonons are related to the corresponding capture rates (given by equations (14) and (20)) by the detailed balance relation,

$$\left(\partial W^{[e]}_{2\mathrm{D}\to 3\mathrm{D}}/\partial E\right)\Big|_E$$
$$= \exp(\pm\hbar\omega_0/T) \left(\partial W^{[e]}_{3\mathrm{D}\to 2\mathrm{D}}/\partial E\right)\Big|_{E\mp\hbar\omega_0}. \tag{21}$$

Here the superscripts e and a stand for 'emission' and 'absorption'. For the (quasi)elastic impurity and DA phonon-mediated processes the capture and escape rates are equal.

In order to estimate the probability for a captured electron to relax via 2D states to the bottom of the QW instead of being emitted to delocalized states, we calculate the rate of LO phonon-assisted transitions between the confined states. Substituting equations (7) and (8) in (12) we obtain

$$\left(\frac{\partial W}{\partial E}\right)^{\mathrm{LO}}_{2\mathrm{D}\to 2\mathrm{D}} = \frac{2e^2m^2\omega_0\mathcal{S}}{\pi\hbar^4\varepsilon^* a} N^{\pm}(\omega_0) \int_0^{\infty} \mathrm{d}q_z$$
$$\times {\sum_{n,n'}}' \frac{\left|M^{q_z}_{n'\to n}\right|^2}{\sqrt{(\pm k^2_{\mathrm{ph}} + \kappa_n^2 - \kappa_{n'}^2 - q_z^2)^2 + 4q_z^2(\kappa_n^2 + k^2)}}. \tag{22}$$

The summation in equation (22) is performed over the available initial and final states n and n', i.e. $-\epsilon_n < E$ and $-\epsilon_{n'} + \hbar\omega_0 < E$. The matrix elements $M^{q_z}_{n'\to n}$ can be obtained from $M^{q_z}_{k_z,p\to n}$ by changing in equation (15) the quantum numbers (k_z, p) to n' and the length $\mathcal{L}$ to a. The explicit form of $M^{q_z}_{n'\to n}$ is given by equation (A2) of the appendix.

3.3. Total transition rates

To find the total capture rate one must specify the carrier distribution function. Below we assume non-degenerate statistics for the unconfined 3D carriers and small occupancy numbers of 2D states near the top of the well to neglect the Pauli factors. The normalized distribution function $f(k)$ for the non-degenerate 3D electrons has the form

$$f(k) = \frac{4\pi^{3/2}}{k_T^3\mathcal{S}\mathcal{L}} \exp\left(-\frac{k^2}{k_T^2}\right) \tag{23}$$

where $k_T^2 = 2mT/\hbar^2$ is the thermal wavevector of the electrons.

Substituting equations (13) and (18) in (12) we obtain the following expression for the capture rates due to the emission (upper sign) and absorption (lower sign) of an LO phonon:

$$W^{\mathrm{LO}}_{3\mathrm{D}\to 2\mathrm{D}} = \frac{2me^2\omega_0 N^{\pm}(\omega_0)}{\sqrt{\pi}\varepsilon^*\hbar^2 k_T^2\mathcal{L}}$$
$$\times \int_0^{\infty} \mathrm{d}k_z \exp\left(-\frac{k_z^2}{k_T^2}\right) \int_0^{\infty} \frac{\mathrm{d}q_z}{q_z} \sum_{n,p} \left|M^{q_z}_{k_z,p\to n}\right|^2$$
$$\times \exp\left[\left(\frac{\pm k^2_{\mathrm{ph}} - k_z^2 - \kappa_n^2 - q_z^2}{2q_z k_T}\right)^2\right]$$
$$\times \Gamma\left[\frac{1}{2}, \frac{(\pm k^2_{\mathrm{ph}} - k_z^2 - \kappa_n^2 - q_z^2)^2 + 4q_z^2 \max(0, \pm k^2_{\mathrm{ph}} - \kappa_n^2 - k_z^2)}{(2q_z k_T)^2}\right]. \tag{24}$$

Here $\Gamma(\frac{1}{2}, u) = \int_u^\infty \exp(-u)\, du/\sqrt{u}$ is a complementary incomplete gamma function.

The total rates of capture due to the quasielastic emission and absorption of DA phonons are equal and given by

$$W^{\mathrm{DA}}_{3\mathrm{D}\to 2\mathrm{D}} = \frac{mD^2T}{2\sqrt{\pi}\hbar^3 k_T \rho s^2 \mathcal{L}} \times \int_0^\infty dk_z \exp\left(-\frac{k_z^2}{k_T^2}\right) \sum_{n,p} \mathcal{A}_{k_z,p\to n}. \tag{25}$$

For the impurity scattering induced capture we find from equations (12), (17) and (21):

$$W^{\mathrm{imp}}_{3\mathrm{D}\to 2\mathrm{D}} = \frac{8\pi m e^4 n_i}{\varepsilon_0 \hbar^3 k_T^2 \mathcal{L}} \int_0^\infty dk_z \exp\left(-\frac{k_z^2}{k_T^2}\right) \times \int_0^\infty d\kappa \sum_{n,p} \left|\frac{\mathcal{I}^\kappa_{k_z,p\to n}}{\kappa}\right|^2 \exp\left[-\left(\frac{k_z^2 + \kappa_n^2 - \kappa^2}{2k_T\kappa}\right)^2\right]. \tag{26}$$

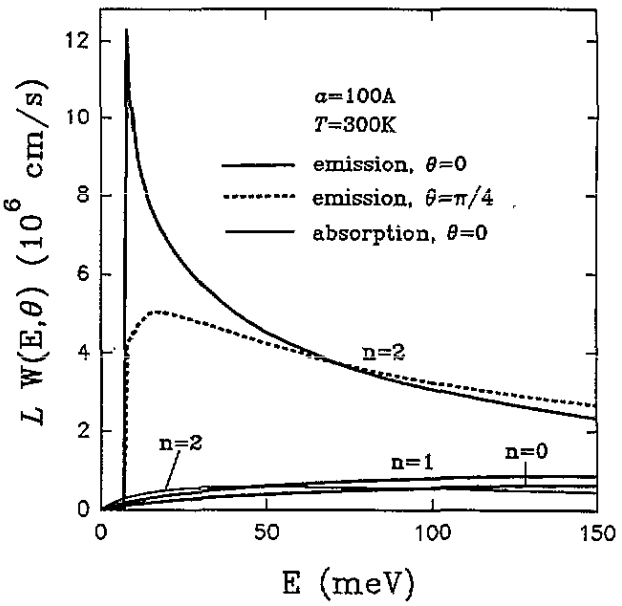

Figure 2. Capture rates, $\mathcal{L}W(E,\theta)$, versus initial electron energy E due to emission (thick curves) and absorption (thin curve) of *polar optical phonons*. Full curves correspond to electron motion perpendicular ($\theta = 0$) to qw and the broken curve to $\theta = \pi/4$. Partial contributions are shown for electron capture from continuum states to the confined states with quantum numbers $n = 0, 1$ and 2 (for phonon emission and $\theta = 0$) or $n = 2$ (otherwise). Width of the well $a = 100$ Å, lattice temperature $T = 300$ K.

4. Numerical results and discussion

We perform numerical calculations for the AlGaAs/GaAs/AlGaAs single quantum well of depth $V_0 = 300$ meV, corresponding to an aluminium content in the barrier equal to $x = 0.33$. We neglect the difference between the other parameters of the well and the barriers and use the material constants of GaAs.

The results of the numerical calculation of the capture rates from the given initial state, W_i, are presented in figures 2–4. We choose the width of the well to be $a = 100$ Å and the lattice temperature $T = 300$ K. For convenience, we performed the summation over the parities p of the initial state, and plotted the dependence of the capture rates on the total kinetic energy $E = \hbar^2(k_\parallel^2 + k_z^2)/2m$ and angle $\theta = \arctan(k_\parallel/k_z)$ of the 3D electron, $W(E,\theta) = \sum_p W_{k_\parallel,k_z,p}$.

Since the wavefunctions of the 3D states are normalized to the distance $\mathcal{L}$ (cf equation (6)), the probability of finding the electron in the vicinity of the quantum well is proportional to $a/\mathcal{L}$ and, as a result, the capture probabilities given by equations (14)–(19) are inversely proportional to $\mathcal{L}$. In order to eliminate the dependence of the final results on the unphysical normalization distance, we plot the 'interface velocity' $\mathcal{L}W(E,\theta)$ with dimensions of cm s^{-1} [11].

In figure 2 we plot the capture rate $W(E,\theta)$ for emission (full curves) and absorption (broken curves) of LO phonons obtained from equation (14). Electrons with energy less than approximately 6 meV cannot be captured to the highest subband ($n = 2$) due to emission of the phonon, because of the energy conservation law.

The relative strength of transition channels is specified by the magnitude of the electron–LO-phonon coupling (8), which is proportional to $1/q^2$, and the dependence of the overlap integral (15) on k_z. Thus, the transitions to the highest subband ($n = 2$), which for the width $a = 100$ Å lies close to the continuum, give the dominant contribution to the capture rates because of small momentum q transferred in the process. Transitions to the lower subbands ($n = 0, 1$) involve larger phonon momenta and the electron–phonon coupling is much weaker. Note that if the width of the well a is slightly increased and the level $n = 2$ becomes unbound, then there will be no capture to the $n = 2$ subband, while the contributions from the deeply lying levels $n = 0, 1$ are practically unchanged. That leads to the appearance of the set of resonances in the dependence of the total capture rates on the width a (cf [4]).

Calculations show that the rate $W(E,\theta)$ initially increases with energy due to the growth of the overlap integral (15), but then drops because of the increase of the effective transferred momentum q. The rapid decrease of the overlap integral for $E \to 0$ is partially due to the pushing of the 3D wavefunction out of the well, which has the following classical interpretation. For a low kinetic energy E the carrier velocity in the barrier is small, but above the well the velocity increases in proportion to $\sqrt{(V_0 + E)/E}$, and the carrier traverses the well in a relatively short time.

The dependence of the rates $W(E,\theta)$ on the angle θ is also specified by the dependence of the overlap

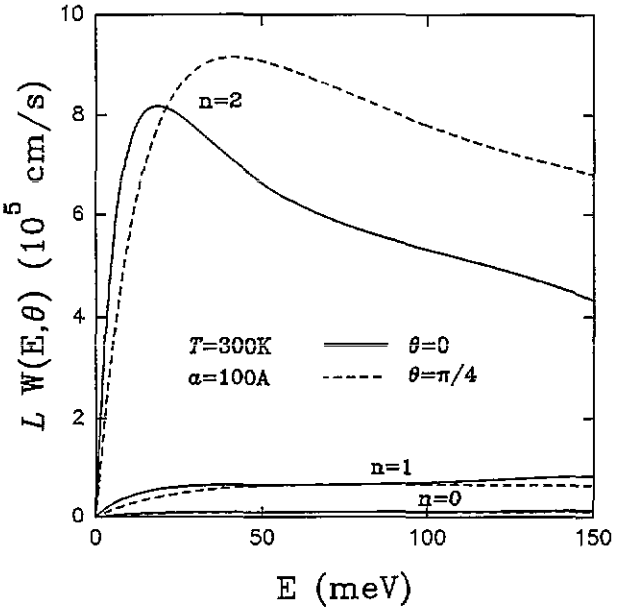

Figure 3. Capture rates, $\mathcal{L}W(E,\theta)$, versus initial electron energy E due to scattering by *impurities* located at both interfaces ($z = \pm a/2$) with a sheet density $n_{imp} = 10^{10}$ cm^{-2} at each interface. Other notations are as for figure 2.

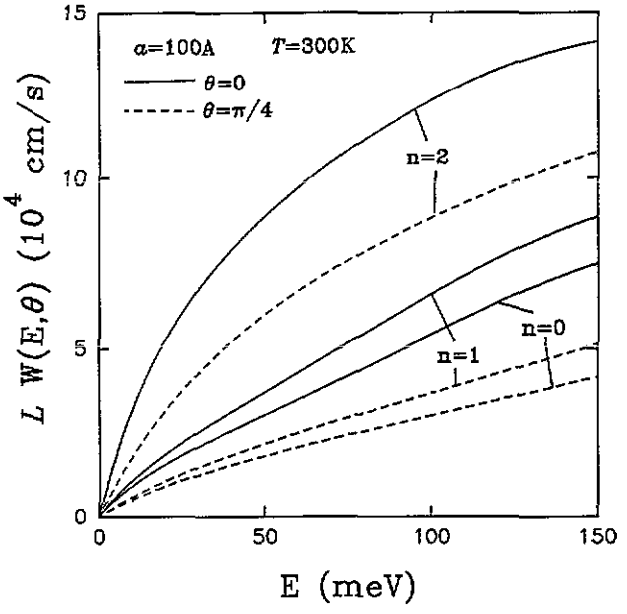

Figure 4. Capture rates, $\mathcal{L}W(E,\theta)$, versus initial electron energy E due to scattering by *deformation acoustic phonons*. Other notations are as for figure 2.

integral (15) on the transverse wavevector k_z. For electrons moving parallel to the interface, $\theta \to \pi/2$, the capture rates $W(E,\theta) \to 0$, because the electrons do not cross the well, and the probability of finding the electron in the vicinity of the well is proportional to $a/\mathcal{L} \to 0$.

Figure 3 depicts the capture rates $W(E,\theta)$ due to scattering by impurities (full curves). The results have been obtained by assuming the sheet impurity concentration $n_i = 10^{10}$ cm^{-2} at each interface. The Coulomb interaction between 3D electron and impurity has the same $1/q^2$ dependence on the transferred momentum as that for LO phonons, which results in a similar rate dependence on energy as in figure 2. Two essential differences with LO phonon-assisted capture are that the impurity scattering is elastic and that the strength of this mechanism (except the resonant condition where a new bound state enters the well) is almost an order of magnitude smaller.

The DA phonon-induced capture rates, $W(E,\theta)$, were calculated with the use of equation (16); note that in the elastic approximation the emission and absorption of the phonon give equal contributions. It is seen from figure 4 that acoustic phonon-mediated capture rates increase much faster with initial electron energy, because the energy of electron interaction with the deformation potential of an acoustic phonon (9), proportional to q, increases with the transferred momentum [18]. However, in contrast to the suggestion in [18], the contribution of acoustic phonons to capture is small for the thermal electrons with energy of order T because of a relatively small coupling constant D.

In order to calculate the net capture rate it is important to know the probability for an already (pseudo)captured electron to relax to the bottom of the well and eventually recombine, rather than to be re-emitted from the well. To answer this question we have

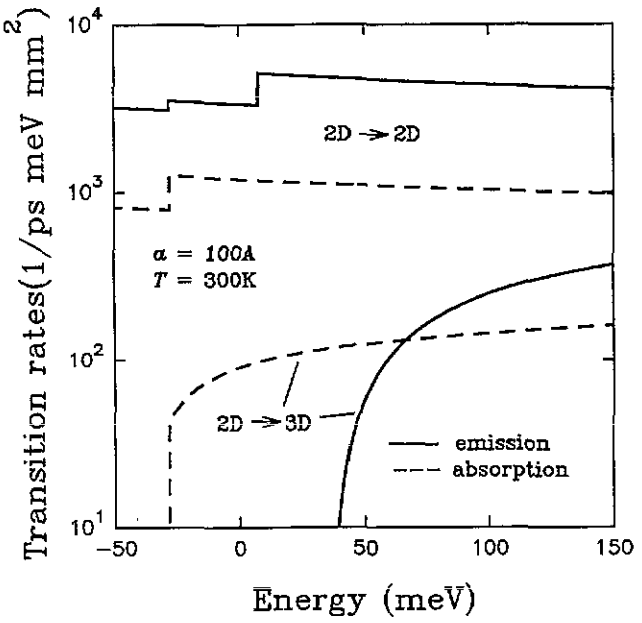

Figure 5. Probabilities per unit energy of transitions within 2D states, $(1/S)\partial W_{2D\to 2D}/\partial E$ (upper part of the figure), and escape probabilities, $(1/S)\partial W_{2D\to 3D}/\partial E$ (lower part of the figure), versus initial electron energy E. Full curves correspond to emission and broken curves to absorption of *polar optical phonons*. Width of the well a = 100 Å, lattice temperature T = 300 K.

calculated the rates of LO phonon-assisted transitions between the 2D states, $\partial W_{2D\to 2D}/\partial E$, given by equation (22), and the rates of escape, $\partial W_{2D\to 3D}/\partial E$, given by equations (21) and (14).

As seen from figure 5, the probability of electron relaxation via 2D confined states due to cascade emission of LO phonons is almost two orders of magnitude higher than that of escape outside of the well (the assumption of non-degenerate statistics and effective electron recombination at the bottom of the well is

essential here). Such a large difference is due to the different density of states for 2D and 3D carriers [19]. The density of states for electrons at a given 2D subband is constant, while for the 3D states it is proportional to $\sqrt{E}$ and becomes comparable to that for 2D states at energies much larger than the electron thermal energy. Thus we may conclude that if the carrier is captured to the well it will not escape, but rather relax to the bottom of the well, and the net capture rates are given by equations (14)–(19).

We plotted the results for the dependence of the capture rates (velocities) $\mathcal{L}W_{3D\to 2D}$, given by equations (24)–(26), on the width of the well a in figures 6–8.

To analyse qualitatively the behaviour of the LO phonon-mediated capture rates with respect to the width of the well a we discuss the case of low temperature, $T = 20$ K, where all the electrons are at energies well below $\hbar\omega_0 \approx 450$ K. Following Brum and Bastard [4], we have calculated the partial contributions for capture to different subbands, $n = 0, 1, 2, 3$ from the symmetric initial states with parity $p = 0$ (figure 6(a)) and antisymmetric states with parity $p = 1$ (figure 6(b)). Only transitions due to emission of phonons are taken into account, because the contribution of phonon absorption is negligible at low temperature.

As we see, there exist two different sets of resonances in the $W(a)$ dependence. The first set occurs when the nth level is at an energy $\hbar\omega_0$ below the barrier, i.e. the ionization energy $\epsilon_n = \hbar\omega_0$. In this situation the 3D electrons with energy $E \sim T \ll \hbar\omega_0$ can emit an LO phonon from the bottom of the 3D conduction band to the bottom of the nth subband. Since the transition occurs between states with small wavevectors k, the transferred momentum q is small and the capture rates increase resonantly due to the $1/q^2$ factor in equation (8). The enhancement of the transition rates owing to the $1/q^2$ singularity in (8) appears to be stronger than the opposite effect caused by a decrease of the overlap integral (15).

The second set of resonant maxima occurs when, with the decrease of the width a, the nth bound state leaves the well [4] (the case $n = 0$ is excluded). Because of the term $\mathrm{cs}_p(k_{wz}a/2)$ in the denominator of equation (6) for the 3D wavefunction, the confined state becomes a virtual resonant continuous state with a greatly enhanced probability of observing the particle within the well. Thus, for $\epsilon_n \approx 0$ most of 3D electrons occupy the resonant state, and the drastic increase in the capture rates occurs because of enhancement of the overlap integral (15).

It is important to note that the resonant virtual state 'inherits' the symmetry of the corresponding bound state [4], i.e. the probability of finding the particle within the well will be enhanced for the state $\psi_{k_z,p}(z)$ with parity equal to that of the state $\psi_n(z)$. The reason is that the minima corresponding to $n = 2, 4$ appear only in figure 6(a) (symmetric 3D states, $p = 0$), and the minima for $n = 1, 3$ appear only in figure 6(b) (antisymmetric initial states, $p = 1$). The probabilities are enhanced for the transitions to all lower-lying

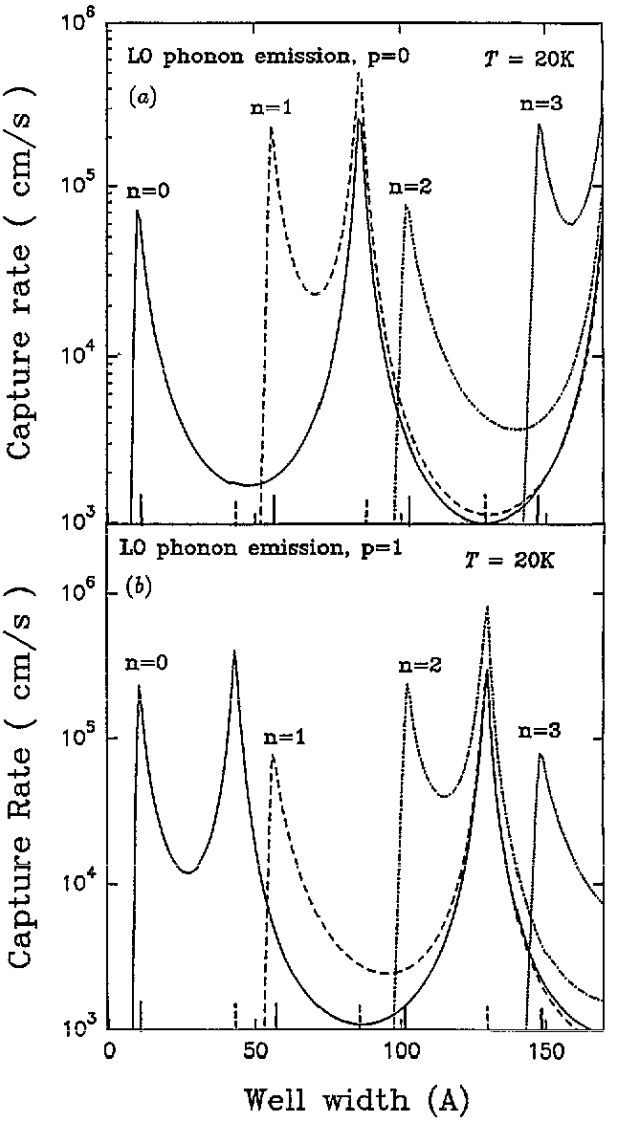

Figure 6. Partial contributions to the total capture rates, $\mathcal{L}W_{3D\to 2D}$ (in cm s^{-1}), due to the *emission* of *polar optical phonons* for different electron final states versus the width of the well a. (a) The symmetric initial 3D state ($p = 0$), (b) capture from an antisymmetric initial state ($p = 1$). Full, broken, chain and dotted curves correspond to final electron states with subband numbers $n = 0, 1, 2$ and 3. Lattice and electron temperature $T = 20$ K.

confined states, and not just a single one, like in the first set of the resonances.

In figure 7 we have plotted the total capture rates $W_{3D\to 2D}$ due to the emission and absorption of LO phonons for three different temperatures, $T = 20$, 77 and 300 K. Both sets of resonances in the well width dependences are very sharp for $T = 20$ K; they become more smeared at $T = 77$ K, and at room temperature only the first set of resonances (at $\epsilon_n \approx \hbar\omega_0$) produces maxima, while the second one (at $\epsilon_n \approx 0$) is practically smeared out.

One can point out that the strength of the first set of resonances ($\epsilon_n \approx \hbar\omega_0$) hardly changes when the temperature is decreased from 77 K to 20 K. This is because when the condition $E \sim T \ll \hbar\omega_0$ is reached, practically all electrons have the same probabilities of emitting a phonon and relaxing to the bottom of the

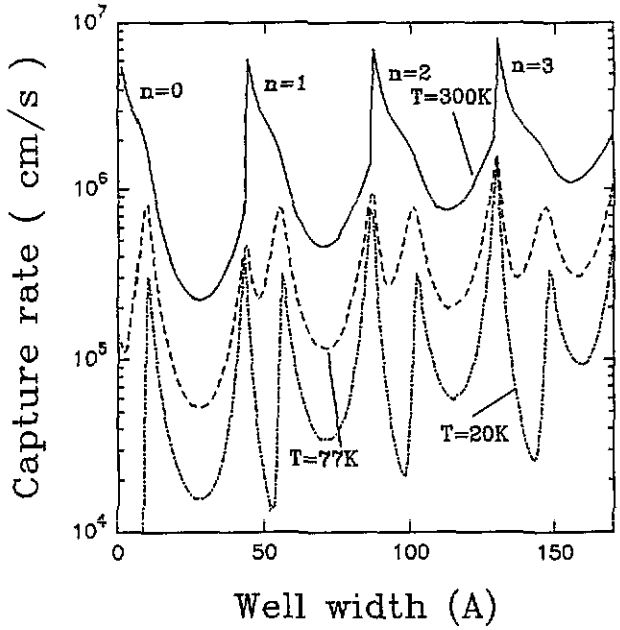

Figure 7. Total electron capture rate $\mathcal{L}W_{3D\to 2D}$ (in cm s^{-1}) due to the emission and absorption of *polar optical phonons* versus the width of the well a. Full, broken and chain curves correspond to the lattice and electron temperature $T = 300$, 77 and 20 K.

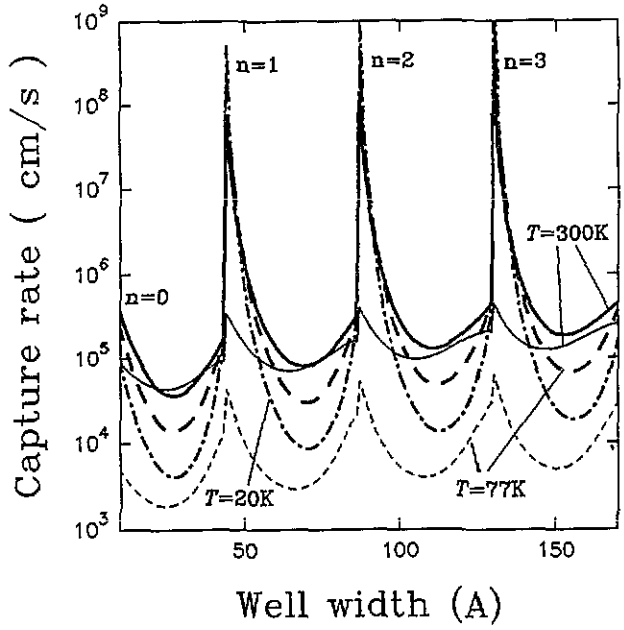

Figure 8. Total capture rate $\mathcal{L}W_{3D\to 2D}$ (in cm s^{-1}) due to scattering by *impurities* (thick curves) and *deformation acoustic phonons* (thin curves) versus the width of the well a. Impurities are located at both interfaces ($z = \pm a/2$) with a sheet density $n_{imp} = 10^{10}$ cm^{-2} at each interface. Full, broken and chain curves correspond to the lattice and electron temperature $T = 300$, 77 and 20 K.

nth subband. On the other hand, the magnitudes of the second set of peaks continue to drop, since at low energy the width of the resonant level is still comparable to the temperature, and the saturation has not yet occurred. Our calculations agree with results reported by Kuhn and Mahler [11] at $T = 10$ K under the assumption of full phase coherence.

Note that in the paper by Brum and Bastard [4], instead of the second set of resonances corresponding to the appearance of a new bound state in the well ($\epsilon_n \approx 0$), resonances of another type are predicted, where the resonant state is at the optical phonon energy above the conduction band edge ($\epsilon_n \approx -\hbar\omega_0$). This is because the authors assumed a degenerate electron distribution with a large Fermi energy (electrons exist at all energies below $\hbar\omega_0$) and considered only the 'true' capture processes with the electron final state below the barrier.

Finally, in figure 8 we show the capture rates due to (quasi)elastic scattering by the interface impurities (thick curves) and deformation acoustic phonons (thin curves). Both dependences have the set of resonant peaks corresponding to the entrance of new levels into the well ($\epsilon_n \approx 0$), due both to addition of the new final 2D states when the nth level is bound (to the right of the resonance) and to an enhancement of the probability of finding the particle in the initial 3D state when the level is virtual (to the left of the resonance).

Similar to the case of the first set of resonances for the LO phonon-assisted capture ($\epsilon_n \approx \hbar\omega_0$), the transferred momentum q is small. That leads to an additional enhancement of impurity scattering and suppression of the acoustic phonon-assisted capture in the vicinity of the resonance. With a decrease of temperature the effective transferred momentum q becomes smaller, the $1/q^2$ and q-like dependence of electron coupling to impurities and DA phonons (see equations (9) and (10)) becoming stronger. This effect and the proportionality of the DA phonon occupation number to T govern the temperature dependence of these two capture mechanisms.

Comparison of figures 7 and 8 shows that LO phonon-assisted capture dominates at all widths, except where the condition $\epsilon_n \approx 0$ is fulfilled. In the narrow vicinity of the well widths defined by this condition, impurity-assisted capture can dominate. Acoustic phonons give a negligible contribution to the capture rates for all parameter ranges.

It should be noted that, because of the domination of the processes with small effective momentum transfer q, the contribution to resonant capture can be given by remote impurities with $q \leqslant 1/\ell$, where ℓ is their distance from the well. On the other hand, at finite electron concentrations and small q the capture rates will be suppressed by a factor of the order of $(1 + q_s/q)^2$, where $q_s = 2\pi e^2 n/\varepsilon_0 T$ is the Debye screening length of the two-dimensional electron gas.

Evidence for an enhanced impurity-scattering-assisted capture to the multi-quantum well (MQW) structures was obtained in recent femtosecond time-resolved luminescence measurements [16]. However, the accompanying theoretical calculations of LO phonon-mediated capture differ significantly from the original works on MQW [6, 11, 21].

In summary, we have calculated the rates of capture, escape and carrier relaxation within the 2D bound states taking full account of quasibound electron states at positive energies due to LO phonon, DA phonon and

impurity scattering. The contribution of the strongly inelastic LO phonon scattering dominates except for well widths a corresponding to the entrance of a new bound state into the quantum well, where the impurity scattering mechanism with small transferred momentum q dominates.

Acknowledgment

This work was supported by NSF and ARO.

Appendix

The form factor for the phonon-assisted transition between the 3D and 2D states (see equation (14)) is equal to

$$M^{q_z}_{k_z,p\to n} = C_n\Bigg((-1)^p \times \frac{(-1)^{np}\kappa_n \mathrm{cs}_n(\varphi+\varphi_p) - (k_z+q_z)\mathrm{cs}_{n+1}(\varphi+\varphi_p)}{\kappa_n^2+(k_z+q_z)^2} + \frac{(-1)^{np}\kappa_n \mathrm{cs}_n(\varphi-\varphi_p) + (k_z-q_z)\mathrm{cs}_{n+1}(\varphi-\varphi_p)}{\kappa_n^2+(k_z-q_z)^2} + \frac{(-1)^{np} a \mathrm{cs}_p(\varphi_p)}{4\mathrm{cs}_n(\kappa_{wn}a/2)\mathrm{cs}_p(k_{wz}a/2)} \times [(-1)^{n+p}\Delta(\kappa_{wn}+k_{wz}+q_z) + \Delta(\kappa_{wn}+k_{wz}-q_z) + (-1)^n\Delta(\kappa_{wn}-k_{wz}+q_z) + (-1)^p\Delta(\kappa_{wn}-k_{wz}-q_z)]\Bigg) \tag{A1}$$

where $\Delta(k) = \sin(ka/2)/(ka/2)$ and $\varphi = q_z a/2$.

The form factor for the transitions between the 2D states is given by

$$M^{q_z}_{m\to n} = C_n C_m\sqrt{\frac{a}{2}} \times \Bigg(\frac{(\kappa_n+\kappa_m)\mathrm{cs}_{n+m}(\varphi) + (-1)^{n+m+1}\mathrm{cs}_{n+m+1}(\varphi)}{(\kappa_n+\kappa_m)^2+q_z^2} + \frac{(-1)^{nm}a}{8\mathrm{cs}_n(\kappa_{wn}a/2)\mathrm{cs}_m(\kappa_{wm}a/2)} \times [(-1)^{n+m}\Delta(\kappa_{wn}+\kappa_{wm}+q_z) + \Delta(\kappa_{wn}+\kappa_{wm}-q_z) + (-1)^n\Delta(\kappa_{wn}-\kappa_{wm}+q_z) + (-1)^m\Delta(\kappa_{wn}-\kappa_{wm}-q_z)]\Bigg). \tag{A2}$$

The form factor for the impurity scattering, defined by equation (18), is equal to

$$\mathcal{I}^{\kappa}_{k_z,p\to n} = C_n\Bigg[\frac{\eta+1}{k_z^2+(\kappa_n+\kappa)^2}[(\kappa_n+\kappa)\mathrm{cs}_p(\varphi_p) - (-1)^p k_z \mathrm{cs}_{p+1}(\varphi_p)] + \frac{(-1)^{np}\mathrm{cs}_p(\varphi_p)}{2\mathrm{cs}_n(\kappa_{wn}a/2)\mathrm{cs}_p(k_{wz}a/2)} \times \Bigg(\frac{\kappa\mathrm{cs}_{n+p}(\varphi_+) + (-1)^{n+p}(k_{wz}+\kappa_{wn})\mathrm{cs}_{n+p+1}(\varphi_+)}{\kappa^2+(k_{wz}+\kappa_{wn})^2} \times (\eta+1) + \frac{\kappa\mathrm{cs}_{n+p}(\varphi_-) + (-1)^{n+p}(k_{wz}-\kappa_{wn})\mathrm{cs}_{n+p+1}(\varphi_-)}{\kappa^2+(k_{wz}-\kappa_{wn})^2} \times (\eta-1)\Bigg)\Bigg] \tag{A3}$$

where $\varphi_\pm = (k_{wz}\pm\kappa_{wn})a/2$ and $\eta = (-1)^{n+p}\exp(-\kappa a)$.

The function $\mathcal{A}_{k_z,p\to n}$, defined by equation (16), is equal to

$$\mathcal{A}_{k_z,p\to n} = C_n^2\Bigg(\frac{1}{\kappa_n} + (-1)^p\frac{\kappa_n\cos 2\varphi_p - k_z\sin 2\varphi_p}{k_z^2+\kappa_n^2}\Bigg) + \frac{aC_n^2\mathrm{cs}_p^2(\varphi_p)}{4\mathrm{cs}_n^2(\kappa_{wn}a/2)\mathrm{cs}_p^2(k_{wz}a/2)} \times [[1 + (-1)^p\Delta(2k_{wz}) + (-1)^n\Delta(2\kappa_{wn}) + (-1)^{n+p}\{\Delta[2(k_{wz}+\kappa_{wn})] + \Delta[2(k_{wz}-\kappa_{wn})]\}/2]]. \tag{A4}$$

References

[1] Lau K Y 1993 *Quantum Well Lasers* ed S Zory (Boston: Academic) pp 217–75

[2] Levine B F 1993 *J. Appl. Phys.* **74** R1
Levine B F *et al* 1992 *J. Appl. Phys.* **72** 4429

[3] Shichijo H *et al* 1978 *Solid State Commun.* **27** 1029
Tang J Y *et al* 1982 *J. Appl. Phys.* **53** 6043
Göbel E O *et al* 1983 *Phys. Rev. Lett.* **51** 1588
Feldmann J *et al* 1987 *Appl. Phys. Lett.* **51** 226

[4] Brum J A and Bastard G 1986 *Phys. Rev.* B **33** 1420

[5] Brum J A *et al* 1986 *Phys. Rev.* B **34** 2381
Blom P W M, Haverkort J E M and Wolter J H 1991 *Appl. Phys. Lett.* **58** 2767
Lam Y and Singh J 1993 *Appl. Phys. Lett.* **63** 1874

[6] Babiker M and Ridley B K 1986 *Superlatt. Microstruct.* **2** 287
Babiker M *et al* 1988 *Surf. Sci.* **196** 422
Babiker M, Ghosal A and Ridley B K 1989 *Superlatt. Microstruct.* **5** 133

[7] Brum J A and Bastard G 1986 *Superlatt. Microstruct.* **3** 51

[8] Blom P W M *et al* 1993 *Appl. Phys. Lett.* **62** 1490
Sotirelis P and Hess K 1994 *Phys. Rev.* B **49** 7543
Preisel M, Mørk J and Haug H 1994 *Phys. Rev.* B **49** 14478

[9] Vergeles M V and Merculov I A 1992 *Sov. Phys. Semicond.* **26** 999 (1992 *Fiz. Tekh. Poluprovodn.* **26** 1784)

[10] Ridley B K 1994 *Phys. Rev.* B **50** 1717

[11] Kuhn T and Mahler G 1988 *Phys. Scr.* **38** 216; 1989 *Solid-State Electron.* **32** 1851

[12] Kan S C *et al* 1993 *Appl. Phys. Lett.* **62** 2307

[13] Feldmann J *et al* 1987 *Appl. Phys. Lett.* **51** 226
Westland D J *et al* 1987 *Appl. Phys. Lett.* **51** 590
Deveaud B *et al* 1988 *Appl. Phys. Lett.* **52** 1886
Deveaud B *et al* 1989 *Appl. Phys. Lett.* **55** 2646
Kersting R *et al* 1990 *Superlatt. Microstruct.* **7** 345

[14] Bimberg D *et al* 1985 *J. Lumin.* **30** 562

[15] Fujiwara A *et al* 1992 *Surf. Sci.* **263** 642
Blom P W M *et al* 1993 *Phys. Rev.* B **47** 2072
Barros M R X *et al* 1993 *Phys. Rev.* B **47** 10951
Muraki K *et al* 1994 *Solid-State Electron.* **37** 1247

[16] Deveaud B *et al* 1993 *Solid State Commun.* **85** 367

[17] Murayama Y 1986 *Phys. Rev.* B **34** 2500
[18] Lent C S and Porod W 1988 *Superlatt. Micostruct.* **4** 77
Porod W and Lent C S 1988 *Solid-State Electron.* **31** 359
[19] Lent C S, Liang L and Porod W 1989 *Appl. Phys. Lett.* **54** 2315
[20] Weber G and Paula A M 1993 *Appl. Phys. Lett.* **63** 3026
Paula A M and Weber G 1994 *Semicond. Sci. Technol.* **9** 730
[21] Kozyrev S V and Shik A Ya 1985 *Sov. Phys. Semicond.* **19** 1024